NORCE Norwegian Research Centre AS
www.norceresearch.no

Snow avalanche detection using Sentinel-1 in Langtang, Nepal

Time series analysis of snow avalanche detections 2015-2021

Authors:

Markus Eckerstorfer, Jakob Grahn

Report 3-2021 NORCE Climate

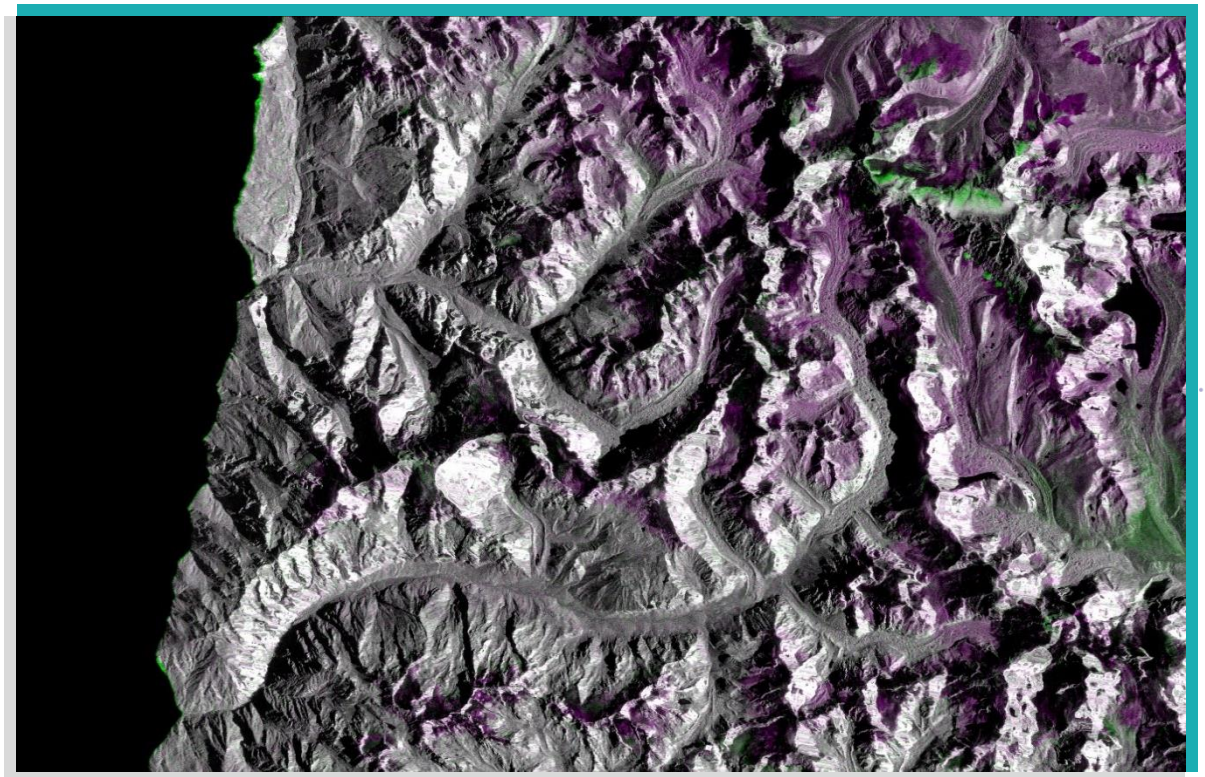

Report title	Snow avalanche detection using Sentinel-1 in Langtang, Nepal
Project No	104127
Institution	NORCE climate and NORCE technology
Client	NVE
Classification:	open
Report No.	3-2021
No. of pages	30
Date of publ.:	September 2021
CC-license	CC BY-NC-SA
Citation	Eckerstorfer & Grahn, 2021, Snow avalanche detection using Sentinel-1 in Langtang, Nepal. NORCE climate report 3-2021.
ISBN	978-82-8408-179-3
Keywords	Snow avalanche detection; snow avalanches; Sentinel-1; radar remote sensing; Langtang; Nepal

Disclaimer

NORCE is not liable in any form or manner for the actual use of the documents, software or other results made available for or resulting from a project and does not warrant or assume any liability or responsibility for the completeness or usefulness of any information unless specifically agreed otherwise in the tender and resulting contract document.

Table of contents

1. Introduction 3
1.1. Scope of this report 3
1.2. Snow avalanche detection using satellite-borne SAR data 3
2. Data and methods 6
2.1. Snow avalanche detection processing system 6
2.2. Spatio-temporal Sentinel-1 data availability 9
2.2.1. Temporal coverage of Sentinel-1 data 10
2.2.2. Spatial coverage of Sentinel-1 data and radar shadow and layover masks 12
3. Results 13
3.1. Feature detection 13
3.2. Snow detections in the Langtang catchment 13
3.3. Snow cover area and snow line altitude in the Langtang catchment 16
3.4. Visual check of RGB change detection images 19
3.5. Comparison of age-tracked detections to ERA5 meteorological variables 21
4. Discussion and conclusion 23
4.1. From detections to snow avalanche activity and the problem of false positives 23
4.2. Snow avalanche activity monitoring using Sentinel-1 in Langtang, Nepal 23
4.3. Snow avalanche regime of Langtang, Nepal 24
References 26
5. Appendix 28

1. Introduction

1.1. Scope of this report

This report summarizes NORCE's contribution to the snowAMP2-project where NVE and ICIMOD are working on cryospheric processes and hazards in the Langtang catchment in Nepal. We contribute with radar satellite-borne snow avalanche detections using Sentinel-1 data. The goal is to establish a multi-year inventory of snow avalanche activity in the Langtang catchment.

In this report, we show the results of Sentinel-1 borne snow avalanche detection and discuss the strengths and weaknesses of the used method. We further explain the processing system and work logic applied and discuss other possible workflows for Sentinel-1 data geocoding and change detection.

We then show a step-by-step process that increases our confidence in the automatic detections being indeed snow avalanches instead of false alarms.

We end with some recommendations on how applicable our methods are to the Langtang catchment and conclude with some basic statements about the snow avalanche regime in the area.

1.2. Snow avalanche detection using satellite-borne SAR data

Snow avalanche detection using satellite-borne SAR data is a relatively young field within remote sensing of natural hazards. In recent years, several groups have developed automatic snow avalanche detection algorithms and validated these algorithms in different mountainous regions worldwide. The main reason for the rapid development of the field is the free availability of high-resolution SAR (synthetic aperture radar) data provided by the Sentinel-1 (S1) constellation. The Sentinel-1 satellites are part of the European Commissions' Copernicus Environmental Monitoring Program.

The use of radar satellite data for avalanche detection is advantageous in many ways (Figure 1). Active radar sensors illuminate Earth's surface using microwave radiation and are thus independent of weather or light conditions. The Sentinel-1 satellites deliver free SAR (synthetic aperture radar) data in a consistent manner, enabling near-real time monitoring of medium sized avalanches almost anywhere on Earth (Eckerstorfer et al., 2016).

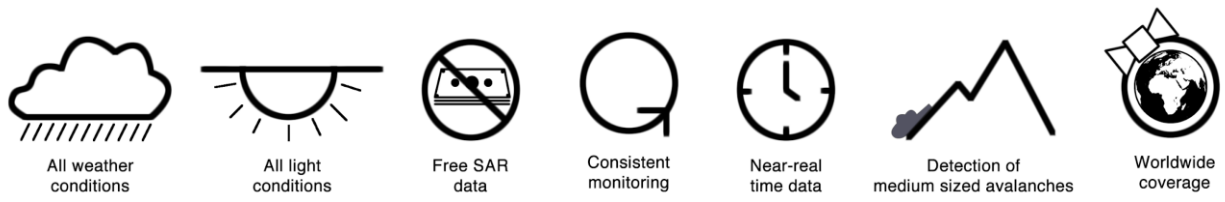

Figure 1: Advantageous characteristics of avalanche detection using Sentinel-1 SAR data.

Satellite-borne SAR detection of snow avalanches is founded on the theory of electromagnetic waves within the radar range interacting with snow-covered ground. Eckerstorfer and Malnes (2015) developed a quantitative model that suggests that snow avalanches exhibit a higher

backscatter than the surrounding, undisturbed snow (Figure 2). Consequently, a handful of studies have utilized this concept, showing that a sharp localized backscatter contrast between snow avalanche debris (the depositional part of a snow avalanche) and undisturbed snow can be detected both by visual interpretation of the SAR images (manual detection), as well as by automatic classification methods. Common to different detection methods, the relative temporal change in backscatter between two SAR images of similar track (e.g. 130) and geometry (e.g. ASC – ascending) is utilized for detection.

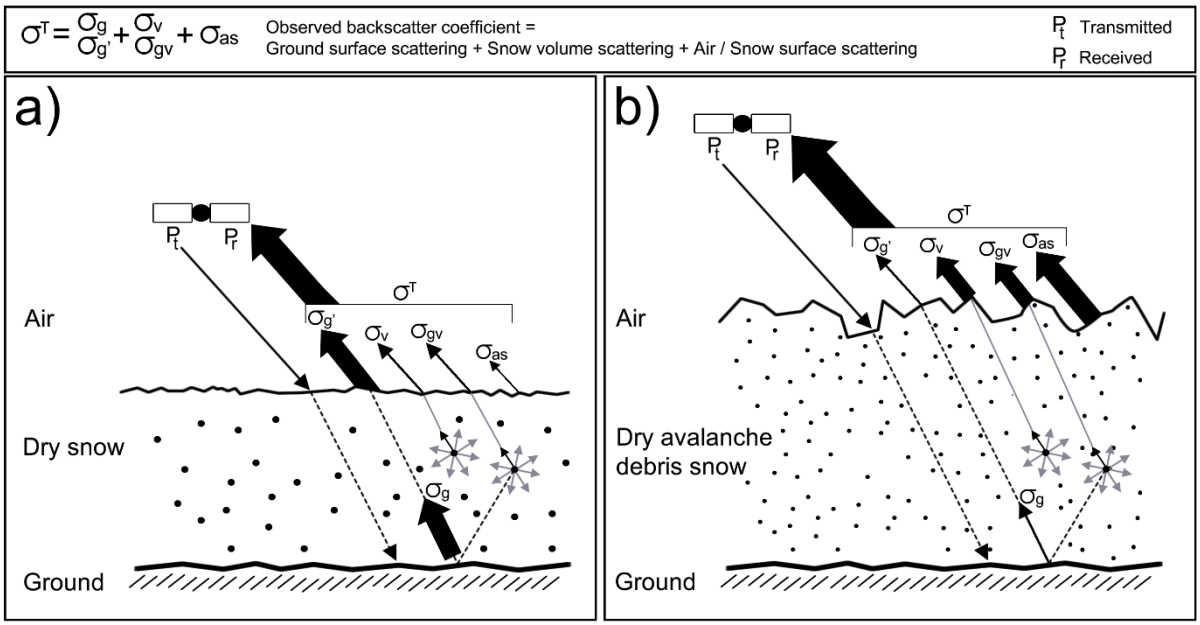

Figure 2: a) Radar backscatter from dry, undisturbed snow, consisting mostly of ground surface scattering. B) Radar backscatter from dry snow avalanche debris. The increased total backscatter is dominated by the contribution from the rough snow surface. Figure modified from Eckerstorfer and Malnes (2015).

The accuracy of SAR borne snow avalanche detection, expressed as probability of detection (POD) and false alarm rate (FAR) is dependent on a number of factors (Figure 3).

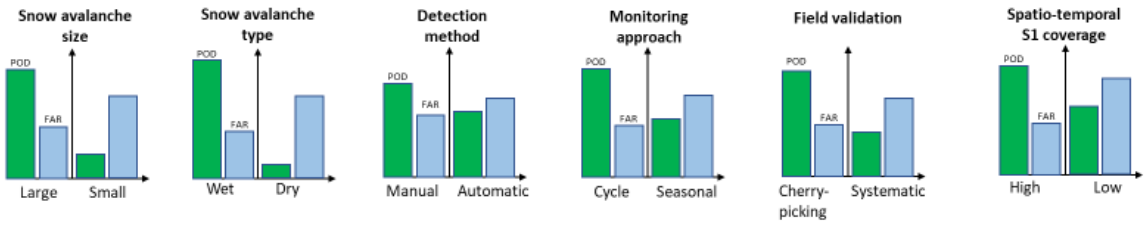

Figure 3: Factors influencing the accuracy of SAR borne snow avalanche detection expressed as POD and FAR. The height of the columns depicts the maximum POD or FAR for each influencing factor based on the available literature.

Most importantly, the spatial resolution of the SAR sensor determines the minimum size of detectable snow avalanches. Several studies have shown that larger snow avalanches are more likely detectable than smaller ones (e.g. Eckerstorfer et al., 2019; Leinss et al., 2020), with POD's over 90 % for large, wet snow avalanches (Eckerstorfer et al., 2019). Snow wetness does therefore also play a role in the detectability of snow avalanches, with wet snow avalanches being more likely

detectable than dry snow avalanches (e.g. Eckerstorfer et al., 2019; Oterhals Daugstad, n.d.). In wet snow, there is no backscatter contribution from the ground surface, thus the relative backscatter difference between rough avalanche debris and undisturbed snow is larger than in dry snow conditions. A recent study by Oterhals Daugstad (n.d.) showed a POD for automatic dry snow avalanche detection of roughly 12 % compared to field-observed snow avalanches. In general, manual detection is still superior to automatic detection methods. However, recent advances in using neural networks for pattern recognition in SAR images are promising (e.g. Bianchi et al., 2020; Sinha et al., 2019; Waldeland et al., 2018). Besides snow avalanche morphology and snow conditions, the spatio-temporal availability and coverage of SAR data plays a role in its usability for snow avalanche activity detection and monitoring. In areas with daily coverage of Sentinel-1 data (e.g. Norther Norway), it is more likely to detect all snow avalanche activity. Areas outside of Europe or high latitudes experience longer repeat cycles or even only Sentinel-1 images of a single geometry (e.g. descending orbit). Finally, higher POD's can be achieved when solely monitoring single extreme snow avalanche events (e.g. Bühler et al., 2019; Hafner et al., 2020) where the extent and magnitude of the activity is known. The detection accuracy certainly decreases with systematic monitoring of an area for an entire or several winters. The same is true also for the applied field validation method. Conducting field observations only after large-scale snow avalanche cycles yields a higher performance than systematic field monitoring throughout a winter, when snow avalanches of different type during different meteorological conditions are recorded.

2. Data and methods

2.1. Snow avalanche detection processing system

For snow avalanche detection in Langtang, Nepal, we used our automatic snow avalanche detection processing system (Figure 4) developed in the SATSKRED project together with NVE. The processing system is comprised of three modules of which the 'initiation module' and the 'avalanche detection and age tracking module' are run separately, however, in consecutive order. Both modules output raster and vector files into the 'output module'. The processing system can be applied to all mountainous areas worldwide that are covered by Sentinel-1 data (see information on data coverage here).

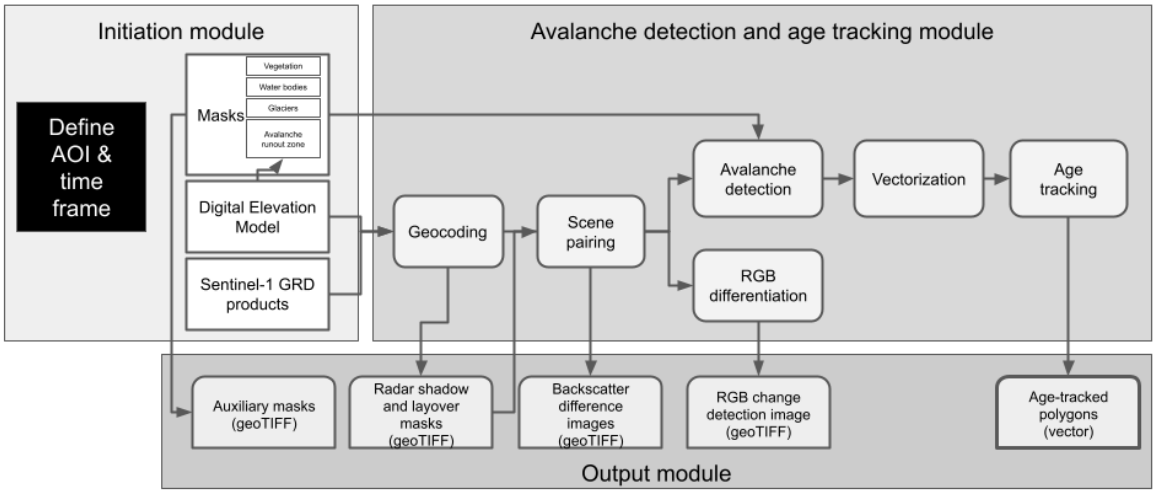

Figure 4: Workflow, data input and data output of the automatic snow avalanche detection processing system

- **Initiation module:** In this module the area of interest (AOI) as a rectangle and the time frame of interest (from 2014 – present is possible) are defined. We defined a rectangular area around the Langtang catchment (see Figure 5) and set the time frame between autumn 2014 (first Sentinel-1 images available) and May 2021 (time of report writing). We downloaded Sentinel-1 (S1) GRD (ground range detected) data in IW mode (interferometric wide swath) for both VV and VH polarization from the Copernicus Collaborative Data Hub (https://colhub.met.no/#/home) for the period 2014/11 – 2021/05. Besides the Sentinel-1 data, a digital elevation model (DEM) is needed for generating an avalanche runout mask and geocode the S-1 data. In this project, we used a 30 x 30 m SRTM DEM (filename: *srtm30_dem.tif*), since the provided, higher resolution DEM had several data holes.

  For snow avalanche detection, besides the radar shadow and layover masks, an avalanche runout mask is the most important input layer (Figure 5). An avalanche runout mask simply defines the area where snow avalanche debris (the detectable part of a snow avalanche) is most likely to occur. We can choose to apply the runout mask pre or post snow avalanche detection. Avalanche runout areas were calculated using an automatic workflow developed by Larsen et al. (2020). The workflow uses potential release areas PRA) (e.g. slope angles between 28 and 60° are considered, in addition to a wind shelter index and terrain roughness) as input and a raster-based hydrological terrain analysis model (TauDEM) that

computes snow avalanche runout lengths based on specific alpha angles. Alpha angles empirically indicate maximum runout lengths of large snow avalanches (Lied and Bakkehøi, 1980). To calculate these avalanche runout areas, an alpha angle of 23° is used. Figure 5 shows the spatial coverage of the avalanche runout mask in both the AOI and in the Langtang catchment, covering 56.1 % of the catchment. We have generalized the runout mask and deleted single isolated pixels as well as summarized large areas using erosion and dilation filtering (filename: *runoutmask_catchment.tif* and *runout_catchment_langtang.shp*). Particularly the second measure prevented the runout mask from dividing detected snow avalanche debris into multiple pieces. In Figure 5 we also show a slope angle classes map with areas outside the avalanche runout areas in green.

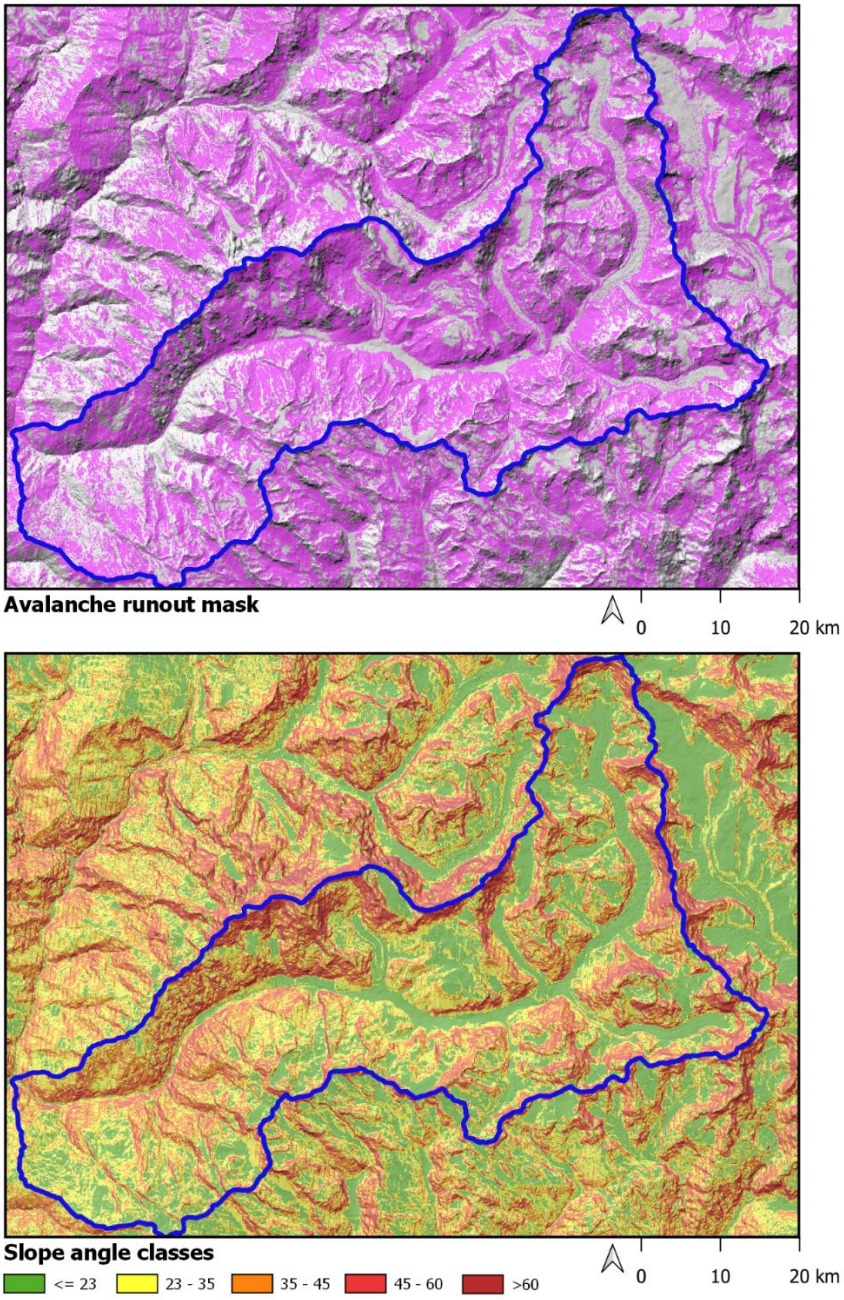

Figure 5: Upper panel: Avalanche runout mask in the Langtang catchment. Lower panel: Slope angle class map of the same area.

Avalanche detection and age tracking module: In this module, the S1 GRD (ground range detected) images are geocoded using our in-house SAR processing software (Larsen et al., 2005). We use GRD products for two important reasons:

- GRD products are about 1/5 the size of SLC (single look complex) products and thus large data quantities are easier to manage.
- GRD products are already radiometrically enhanced, eliminating the need for a single-look complex to multi-look detected processing step on our side

Our geocoding routine is very similar to SNAP or other SAR processing software. We are applying a proper precision geocoding, with an accuracy limited only by orbit and DEM accuracy, and precision limited by the quality of the resampling kernel (which is a performance / precision tradeoff). Our geocoding routine has essentially four steps:

- Start with the required output map projection (usually UTM) and the best available DEM (SRTM in many cases, or national DEMs if available), projected to the required output grid if necessary.

- Solve range-doppler equations with respect to radar slant range/azimuth coordinates for the grid of 3D positions corresponding to the output grid.

- Convert slant range coordinates to ground range coordinates using the product annotations.

- Resample using calculated precise ground range/azimuth coordinates (after converting to subpixel positions in the GRD grid).

- Export $\Delta\sigma$ (radar backscatter) for VV and VH-polarization. Radar backscatter is exported as two separate geotiff-files for the area of interest (rectangle defined for each study area). In addition, we also export a mask-file defining the layover and shadow regions. The images are roughly 20 - 30 mb in size. For this case study, it took roughly two days to geocode all available images.

We essentially are not doing any technical co-registration procedure as all data is geocoded to the exact grid, thus making this step not necessary. Our geocoding is accurate to sub-pixel scale; thus, we can relate pixel to pixel between two different images. Such a geometric process is largely dependent on the accuracy of the DEM used for geocoding. A DEM error is constant in time, so it does not have any effect on pairing of S1 images for change detection, only for absolute positioning.

Snow avalanche detection is a multi-step process. As input, the backscatter difference images in VV and VH polarization are used together with a radar shadow and layover mask and the avalanche runout mask. While the detector discards areas covered by radar shadows and layovers, it looks for snow avalanches in the avalanche runout mask. The images are tiled into 500 x 500 px tiles and three separate steps are performed: a) Difference of Gaussians filtering (DoG) and b) segmentation, with the results of these two stops being combined after c) feature filtering.

a) DoG filtering: We apply two thresholds to the two DoG filtered (ΔVV, ΔVH) images; a lower threshold is defined by μ + 1.5sd and an upper threshold μ + 2.5sd. This yields two interpretations of potential snow avalanche debris pixels, with the result from the higher threshold representing greater likelihood of correct detections.
b) Segmentation: The four input images are segmented into *N* classes and used to calculate a class change (i.e. classified activity image - classified reference image) image for the two channels. To distinguish potential snow avalanche pixels a threshold is calculated automatically (as with the DoG filtering) from the mean and standard deviation of class change values in the image

window. This is done separately for the VV and VH channels. Snow avalanche debris pixels are those that exceed the threshold in each polarization and a binary map (detected features map) is created indicating either 0 for “not snow avalanche” or 1 for “snow avalanche”.

c) Feature filtering: First, the detected regions from the lower DoG thresholding are taken as a proxy for the snow avalanche debris. The number of pixels within each region that were also detected from class change thresholding is deduced and converted into a fraction k_{CC} of the total number of pixels within the region. The fraction of pixels within the region that also exceeded the upper DoG threshold, k_{DoG} is also calculated. If both fractions exceed a specified threshold (k(DoG = 0.3; k(CC) = 0.5)) then the entire detection region is retained; if the criteria are not met, then the detection is nulled out and not considered snow avalanche debris. More information on the algorithm is provided by Vickers et al., (2017).

The final step of the processing system is ‘age tracking’, which essentially deletes snow avalanches that have been detected multiple times in different S-1 images. In that process the shape of the detected snow avalanche is updated (if there is an overlap of over 40 %), however, the date of first detection is retained (Eckerstorfer et al., 2019).

Output module: The ‘age tracked’ snow avalanche detections in vector format are the main output of the processing system. Each detected snow avalanche is represented by a vectorized area with meta-information on date and time of detection, morphological (e.g. extent, size) and topographical parameters (e.g. slope angle, slope aspect), as well as information on backscatter for different polarizations. The list of parameters is given in the appendix. Otherwise, auxiliary data such as the different masks as well as RGB change detection images for visual checking are outputted as geotiff files and as jpg files.

The RGB change detection images show the difference in backscatter between two S-1 images of similar track (e.g. 019) and geometry (e.g. DES) within a single repeat pass (e.g. 6 or 12 days). As a side product, used for manual checking, the backscatter difference images are visualized as RGB composites, where relative temporal change in backscatter is colorized.

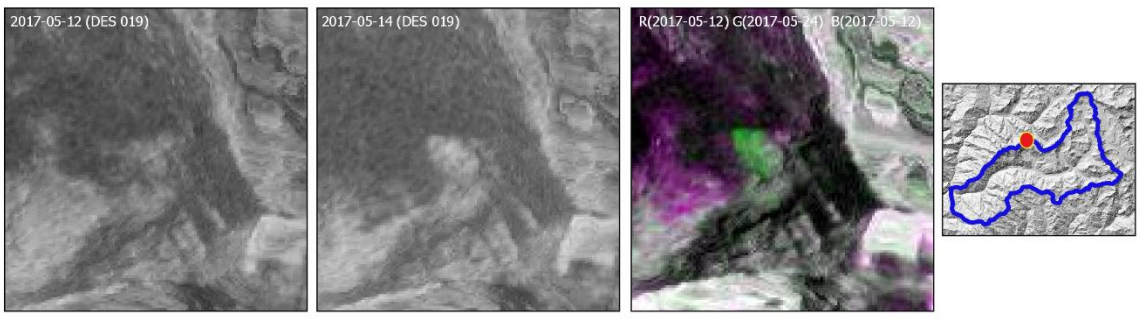

Figure 6: Logic of relative temporal change detection. Left panel: Single backscatter image from 2017-05-12. Middle panel: Single backscatter image from the same path (DES 019) 12 days later with a snow avalanche debris visible. Right panel: RGB composite showing colorized relative temporal backscatter change. Green exhibits a relative backscatter increase (in case of snow avalanches), purple exhibits a relative backscatter decrease (in case of wet snow) and grey exhibits no relative backscatter change.

2.2. Spatio-temporal Sentinel-1 data availability

The Langtang catchment is covered by three different Sentinel-1 tracks. Track 085 is an ascending track (towards the North Pole) and tracks 019 and 121 are descending tracks (from the North Pole)

(Figure 7). The radar shadow and layover mask for the three tracks are provided as geotiff files (filename: e.g. *radarmask_catchment_019.tif and radarmask_19_langtang.shp*).

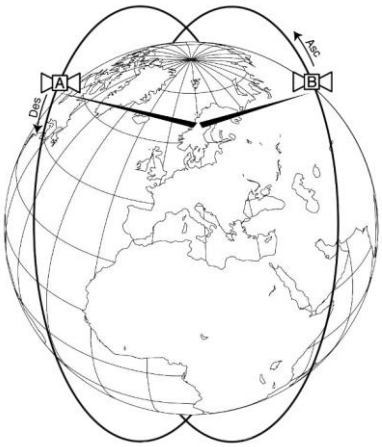

Figure 7: Polar orbits of the Sentinel-1 satellite constellation and the side-looking geometry of the radar sensors.

2.2.1. Temporal coverage of Sentinel-1 data

There was a single Sentinel-1 image available from 28 February 2015 (019 ASC) (not shown in Figure 8). However, systematic acquisition of Sentinel-1 images over Langtang started in October 2016. Until 10 May 2021, 350 Sentinel-1 images were acquired and used for snow avalanche detection. The repeat pass cycle for the three available tracks is 12 days, however, there are considerable data gaps especially for tracks DES085 and DES019, with ASC121 being the most consistently acquired track. These data gaps mostly occurred during the summer months and are likely due to ESA deciding on switching of the SAR sensors over the Himalayas for certain periods.

To put the acquisition pattern for Langtang into perspective, in central Norway, we were able to acquire 504 Sentinel-1 images from four geometries (two ASC and two DES) over four consecutive winters. On the other hand, we conducted a test in Colorado, USA in 2018, where only one descending track with a 12-days repeat pass was available over the AOI.

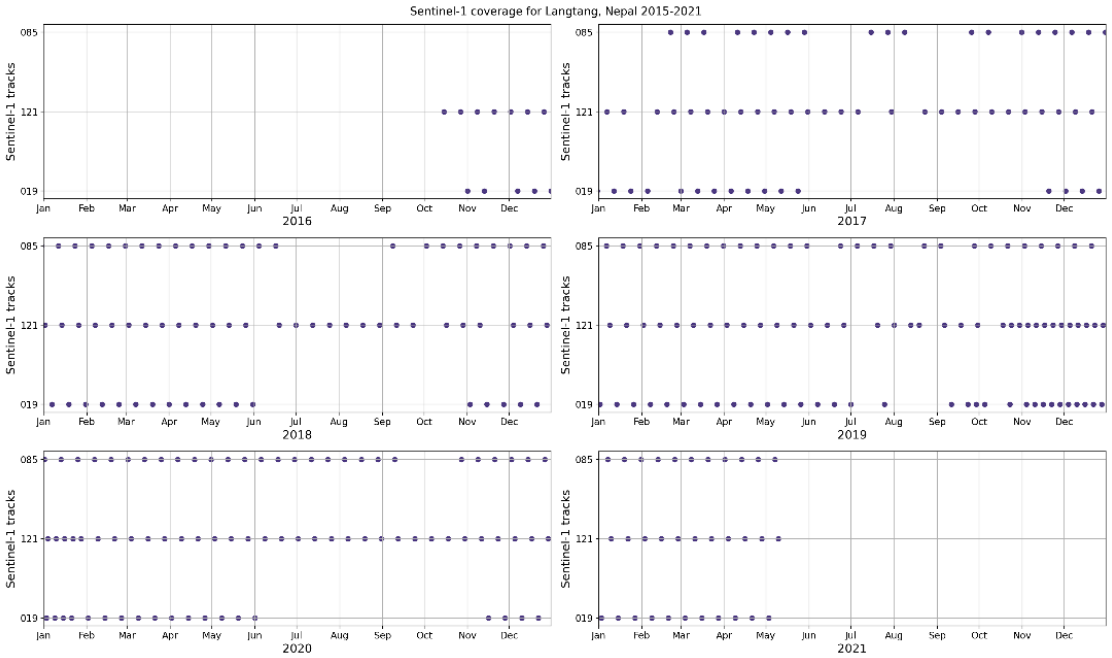

Figure 8: Temporal resolution of Sentinel-1 data in the period 2016 – 2021 divided by Sentinel-1 tracks and calendar years.

A complete temporal acquisition pattern within a 12-days repeat cycle in the Langtang catchment looks as follows (Figure 9): A DES085 image on day 1 (12:22 UTC), followed by a ASC121 image on day 3 (00:11 UTC), followed by a DES019 image on day 8 (00:19 UTC). After a gap of 5 days, the cycle repeats itself with a DES085 image. This means that there is both an uneven distribution of ascending and descending images (2 DES vs 1 ASC) as well as an uneven temporal distribution of Sentinel-1 images with gaps ranging from 2 to 5 days. This is obviously not ideal, however, considering that Nepal is not a top priority for the Copernicus environmental monitoring program, the S-1 availability is satisfying.

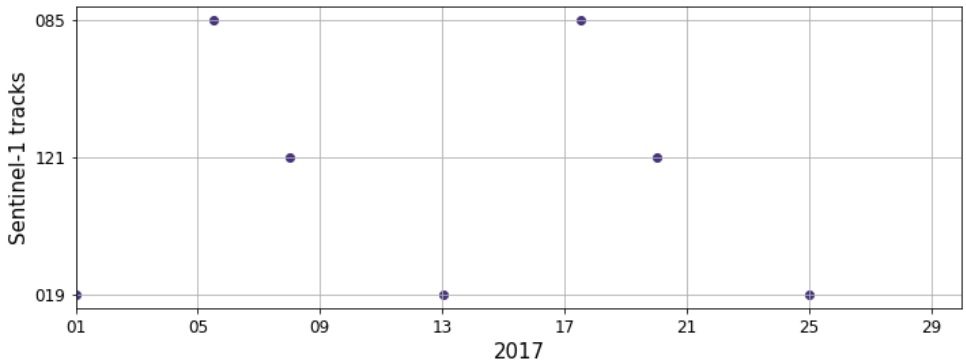

Figure 9: Temporal resolution of Sentinel-1 data within a 12-days repeat cycle.

2.2.2. Spatial coverage of Sentinel-1 data and radar shadow and layover masks

In Figure 10 we show examples of the three available Sentinel-1 image tracks available for the Langtang catchment. Track ASC121 does not cover the most south-western tip of the catchment, the other two descending tracks cover the area completely. Since the SAR sensors on board the Sentinel-1 satellites are side-looking instruments (incidence angle of 29°- 46° with regard to a vertical plane), radar shadow and layover areas occur in mountainous areas When a layover effect occurs, the top of steep mountains tilts and displaces towards the radar sensor from its true position on the ground and distorts the image. When a shadow effect occurs, a mountain side facing away from the radar casts a shadow, as the radar cannot 'see' through the mountain. In these areas, no usable information can be retrieved.

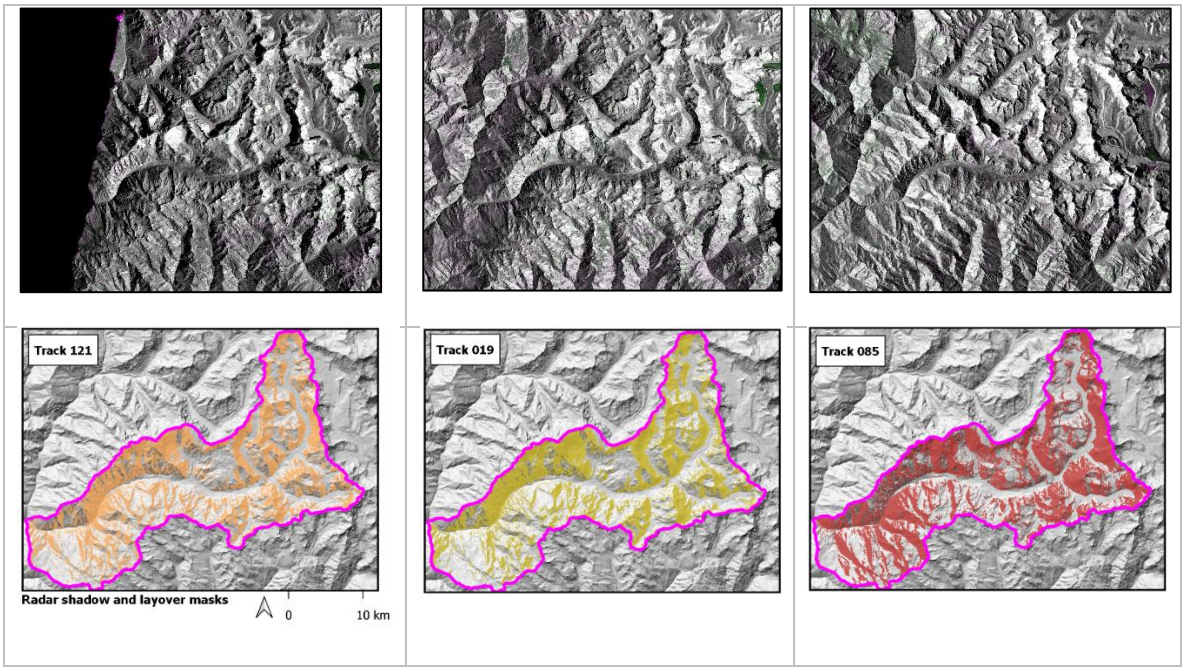

Figure 10: Examples of the three available Sentinel-1 image tracks and the spatial coverage of associated radar shadow and layover masks in the Langtang catchment.

During an ascending track, the radar looks to the right (easterly direction), while during a descending track, the radar looks to the left. Accordingly, areas affected by radar shadows in DES019 and DES085 images are mostly on east, south-east facing slopes, while west, north-west facing slopes are affected by radar shadows in ASC121 images. This means that there is no information available for the snow avalanche detector in these affected areas and they are thus masked out. The total area of the Langtang catchment is roughly 585 km^2. The radar shadow and layover masks cover this area with 44 % (ASC121), 48 % (DES085) and 43 % (DES019) respectively (Figure 10).

3. Results

3.1. Feature detection

Within the defined rectangular AOI, the snow avalanche detector detected 10212 features (Figure 11) (filename: *detect_agg_all_norunout.shp*). These features have not undergone 'age tracking', thus also multiple detections are shown. We have also not applied the avalanche runout mask during avalanche detection. In areas that we are not familiar with, it makes sense to get an impression of what the avalanche detector considers as 'snow avalanche'. In a visual examination of the detections we identified elongated, across-slope features (Figure 11a) that mark the edge of track ASC121 that does not cover the western part of the AOI. In Figure 11b we show detections at or near a mountain top which is rather unlikely. Figure 11c shows elongated features in the valley bottom that are likely due to a river that might freeze and thaw. Finally, Figure 11d shows small features in the middle of a glacier. The SAR signal on a glacier is highly dynamic, especially above the firn line. Moreover, it is unlikely that such small 'snow avalanches' occur at or beyond the maximum extend of the runout zone.

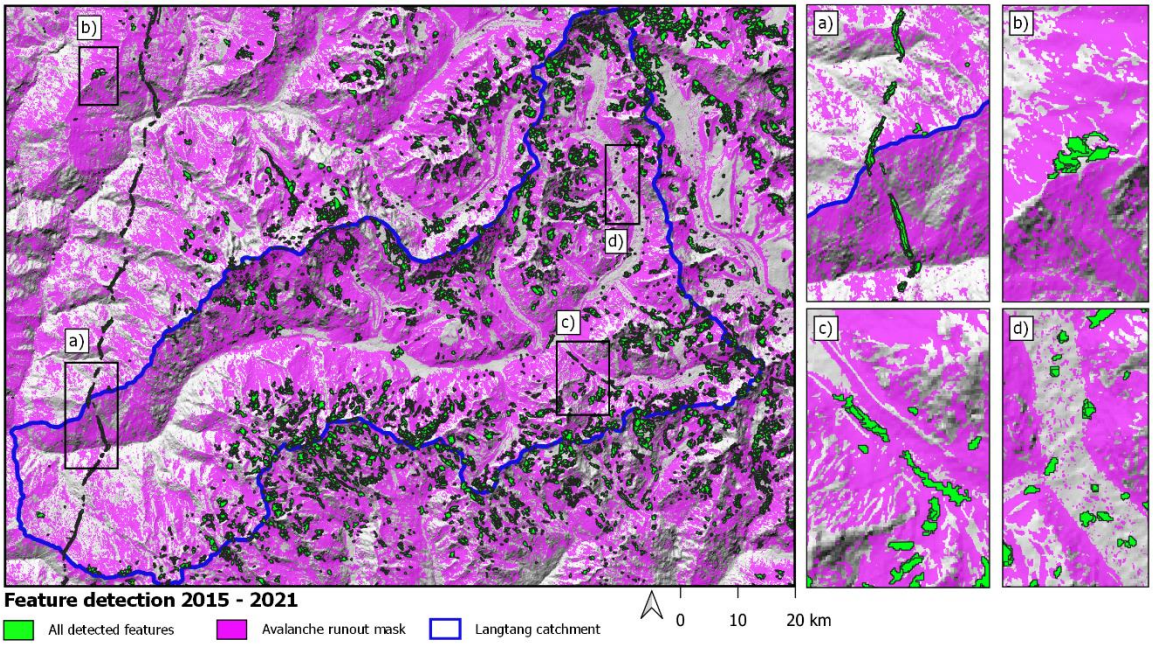

Figure 11: Feature detection map 2015 – 2021 showing all detected features (green vector shapes) in the rectangular area of interest encompassing the Langtang catchment (pink line).

3.2. Snow detections in the Langtang catchment

To arrive at the map of snow avalanche detections presented in Figure 11, we carried out four steps. We deleted all detections outside the Langtang catchment, we deleted the elongated features shown in Figure 11a and we applied the avalanche runout mask, deleting all features outside of the masked area. Finally, we applied our 'age-tracking algorithm, deleting multiple detections. The latter two steps are normally done automatically in the processing system.

All detections within the Langtang catchment amounted to a total to 5892. After 'age-tracking', 2716 detections remained, which we show in Figure 12 (filename: *Avl_detect_agg_langtang.shp*). As a

first impression, most detections are at high elevations close to the ridge lines. Furthermore, there is an absence of detections in the western part of the Langtang catchment which might be a result of the area being covered by two out of three S-1 tracks, as well as their lower elevation compared to the rest of the studied area.

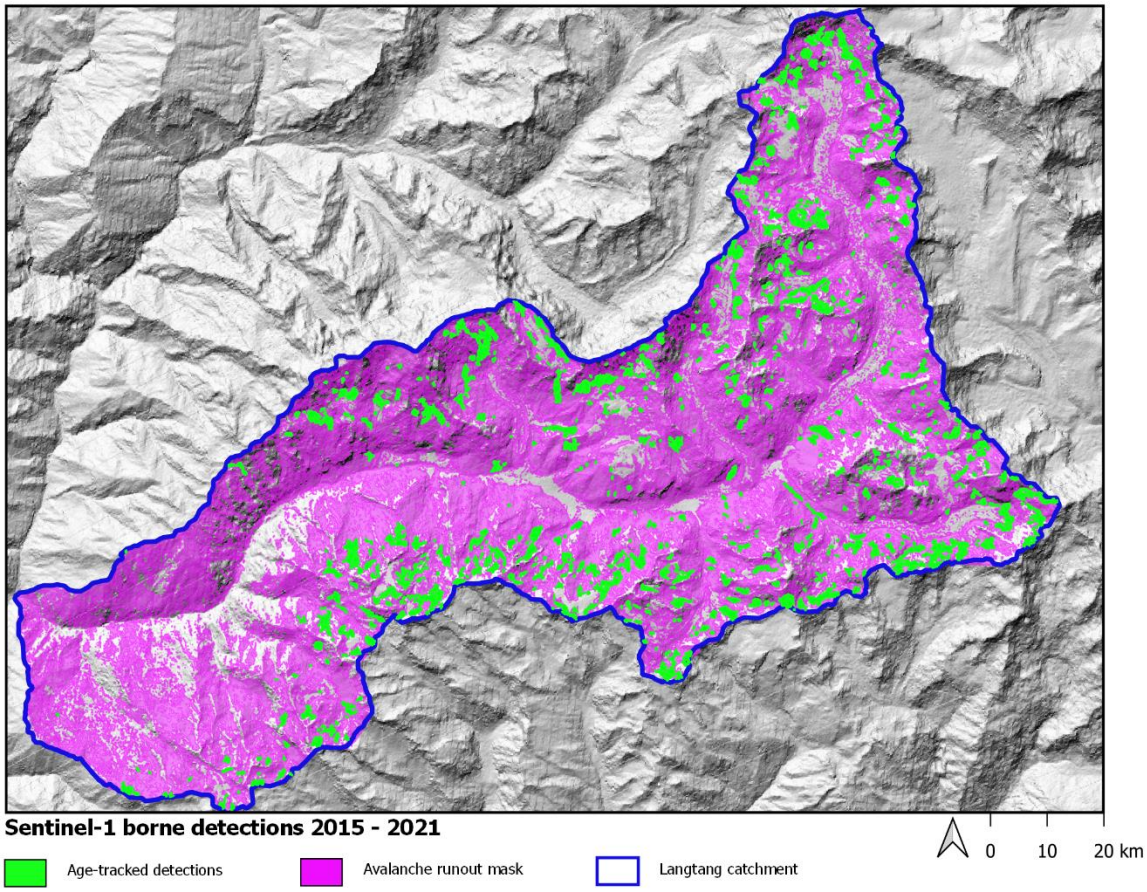

Figure 12: Map of Sentinel-1 detected snow avalanche activity 2015 – 2021 in the Langtang catchment

In Figure 13 we show annual time series of daily detections in the period 2016 – 2021. The bar charts show both 'all detections' (purple) and the reduction in daily detections through 'age-tracking' (green) effectively deleting multiple detections. Without knowledge about the snow conditions – and thus increased certainty if these detections are snow avalanches – a seasonal pattern of detections emerges. During a given year, peak periods of detections nestle around the period April – June and October – December (Figure 13).

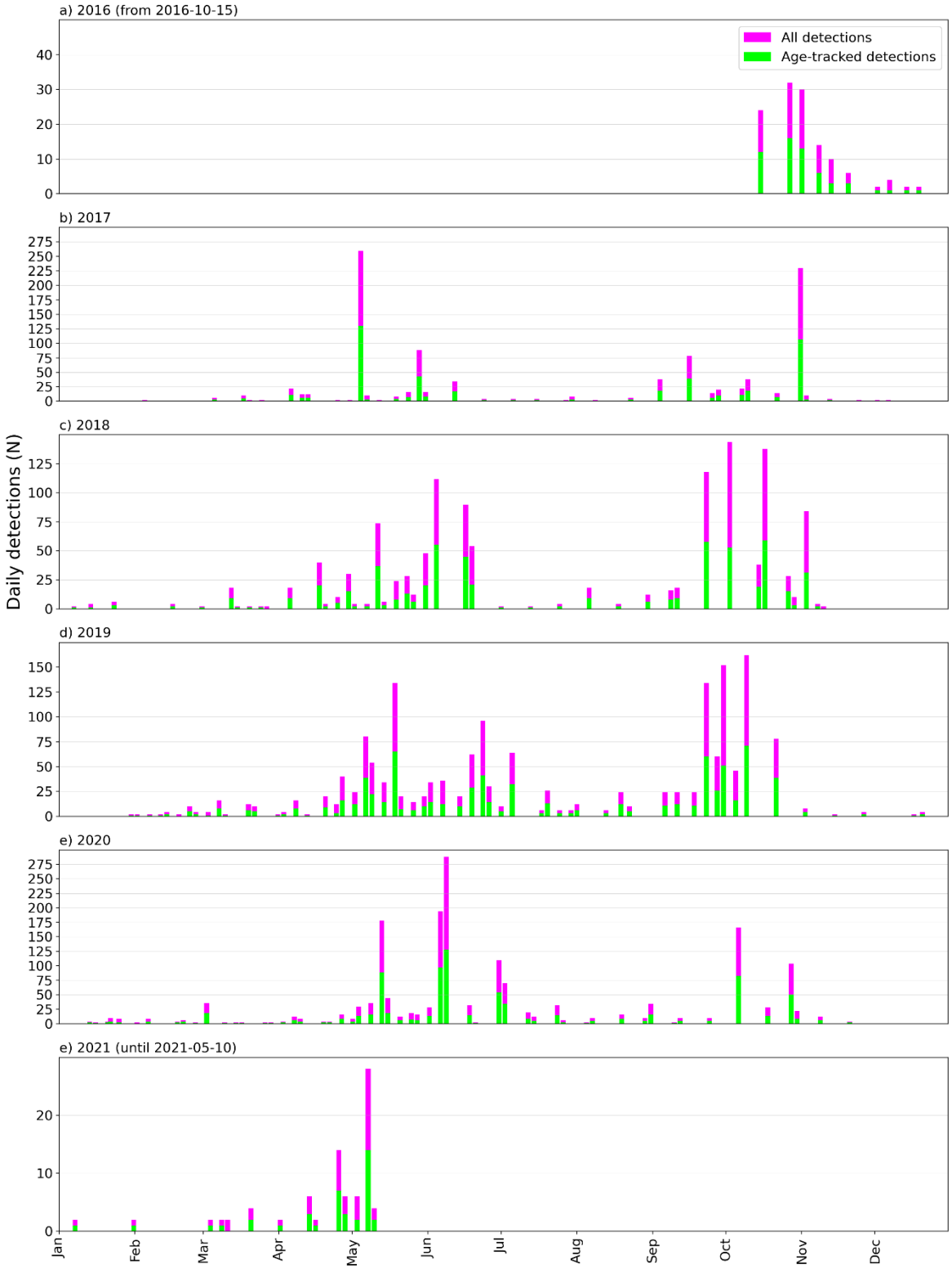

Figure 13: Annual time series of daily detections for both 'all detections' and 'tracked detections' in the period 2016 – 2021. Note the different scale of the y-axis for each year. Note furthermore that the first detection was done 15 October 2016 and the last detection was done 10 May 2021.

More than 80 % of the age-tracked detections were between 4000 – 35000 m^2 large which roughly translates to a majority of size 2 and 3 avalanches (Figure 14). Note that there is a minimum size

cut off at 4000 m^2 to avoid too many false alarms. We furthermore see a typical distribution of slope angles at the maximum runout (which is the minimum elevation shown in Figure 15) averaging around 15-18 degrees and an average maximum runout elevation of roughly 5000 m asl.

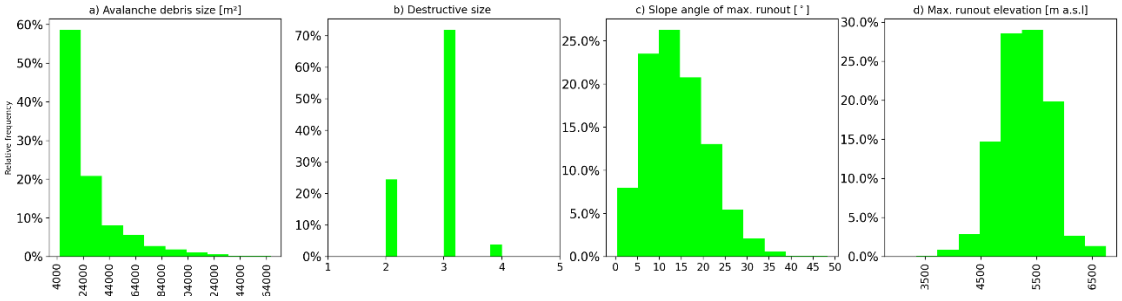

Figure 14: Histograms of morphological and topographical parameters of age-tracked snow avalanches

3.3. Snow cover area and snow line altitude in the Langtang catchment

Khadka et al., (2020) used MODIS data to study the dynamics of snow cover area (SCA) and snow line altitude dynamics (SLA) in Nepal in the period 2003 – 2018. Maximum SCA over central Nepal (including Langtang) was observed in February, with the highest average SCA generally at the turn of the winter season to the pre-monsoon (Jan – Apr). Minimum SCA was observed in the post-monsoon season, typically in October – November. The authors also found an elevation dependency of the SLA with areas over 4500 m asl. largely covered in snow also in the post-monsoon season. The SLA was derived from the post-monsoon SLA, which resulted in an SLA for central Nepal of approximately 4750 m asl. There is, however, probably an uncertainty of +- 500 m, given the 500 m pixel resolution of MODIS data. The study concluded with showing a negative trend for the SCA and a slight upward shift of the SCA that, however, experiences large interannual variability.

Simply based on the elevation dependency of seasonal snow in the Langtang catchment, we present the minimum elevation of all detections over time in Figure 15 and show it in a map in Figure 16. During and slightly after the periods with maximum snow cover (March – June and October-November), detections were located also below the regional SLA of 4750 m asl., reaching as low as roughly 3000 m asl. which constitutes the valley floor in the central part of the Langtang catchment. Thus, based on this simple analysis, all detections are retained for further analysis.

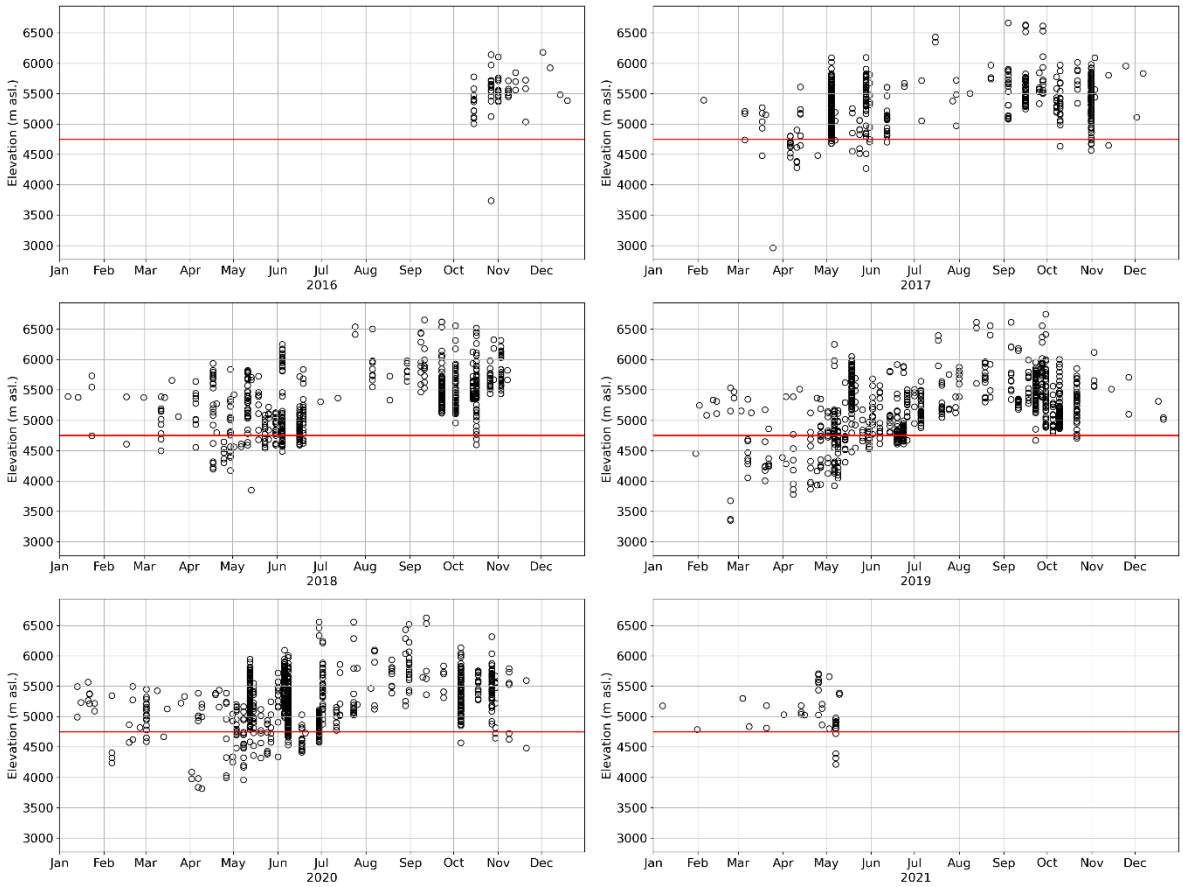

Figure 15: Annual time series of daily detections according to the minimum elevation of the detected polygons. The red lines indicate the regional SLA of 4750 m asl.

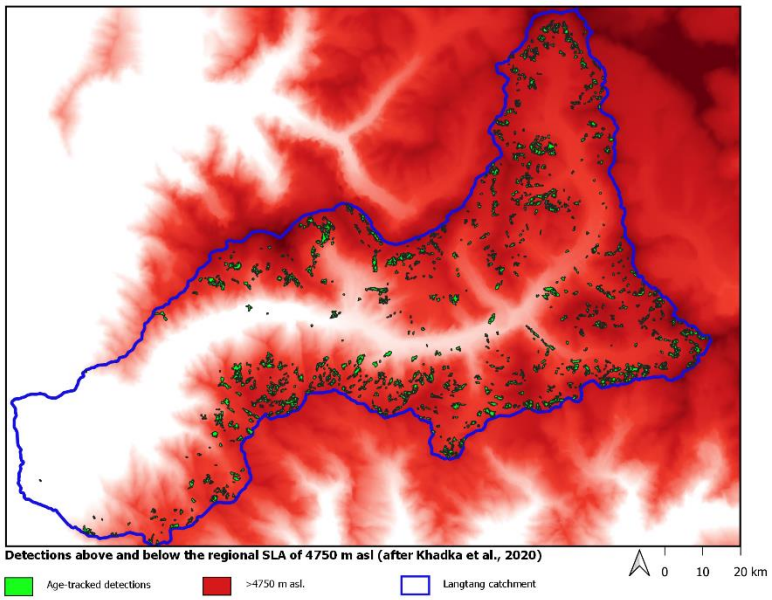

Figure 16: Map showing elevations above 4750 m asl. in red with age-tracked detections superimposed.

Muhammad and Thapa (2020) provide daily MODIS products with 500 m spatial resolution, available through a Pangaea data repository (Muhammad, 2020) for the period 2002-2019. Unfortunately, a systematic analysis on detections being within a snow-covered pixel failed due to the following reasons:

- The temporal uncertainty of the detections of maximum 6 days leads problems when matching them to MODIS products.
- The MODIS products are averaged over 8 days, complicating further a temporal match-up with the detections.
- The MODIS time series does not cover the time series of detections

We thus refrain from masking out detections that are not within pixels classified as snow-covered in the MODIS products. Also, a visual check of initial results did not always make sense as for example shown in Figure 17 and Figure 18. It makes sense that the MODIS products indicate snow cover at higher elevations. However, at the same time, the SAR image indicate a potential change from wet to dry snow (greenish tone) at many locations where MODIS did not indicate a snow cover.

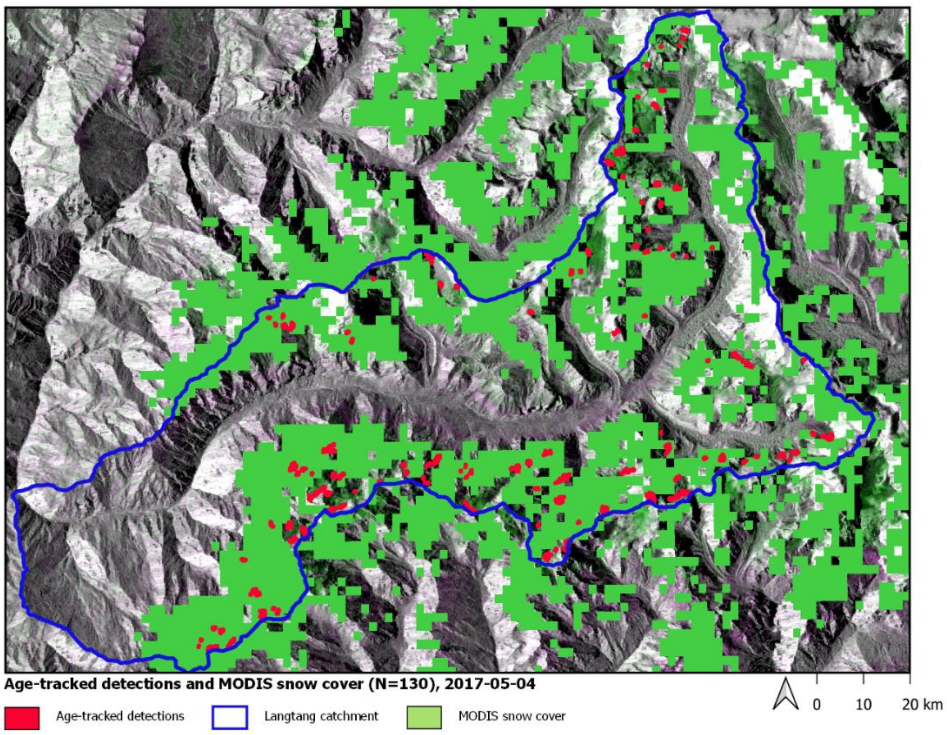

Figure 17: RGB change detection image from 4 May 2017 with MODIS snow cover and age-tracked detections superimposed.

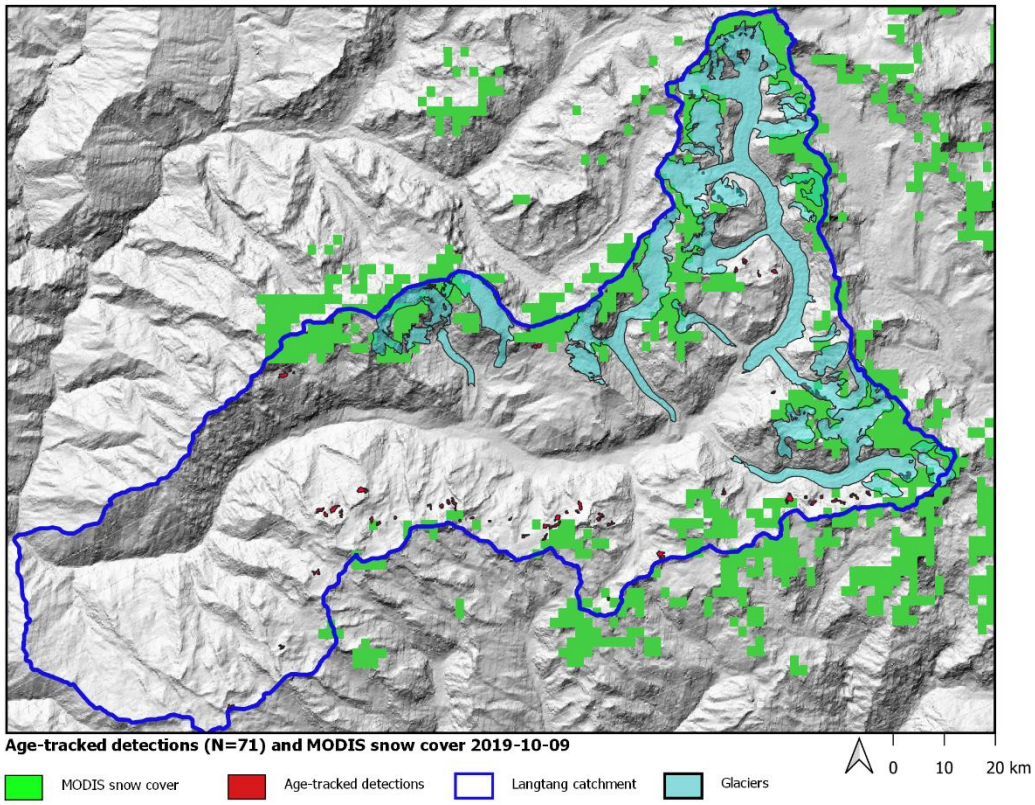

Figure 18: RGB change detection image from 9 October 2019 with MODIS snow cover and age-tracked detections superimposed.

3.4. Visual check of RGB change detection images

We conducted visual checks of the RGB change detection images containing high daily detections. Amongst others, the images from 4 May 2017, 31 October 2017, and 8 June 2020 had 130, 128, and 107 detections respectively. Common to these images, and others with a relatively high amount of detections, large areas with a green tone appear, which indicates that backscatter has increased between the two image acquisition dates that the RGB change detection image is composed of. If localized, in a typical tongue-shape and inside the avalanche runout mask, these areas of backscatter increase are associated with avalanche debris.

However, as visible in the example given in Figure 19 from 31 October 2017, these green areas of relative backscatter increase are fairly extensive, mainly affecting higher grounds close to ridge lines. We assume that these areas are covered with perennial snow which turned from wet to dry, leading to backscatter increase. In Norway, we are seeing this phenomenon mostly above the firn line of glaciers. In Langtang the glaciated areas are not affected which we attribute to their debris coverage.

What becomes also quite clear from the example in Figure 19 is that such situations unfortunately lead to a very high false alarm rate. From visual interpretation of the detection results, no clear snow avalanche outline can be discerned. A possible work around would be to also create wet snow detection maps that help mask out these periods with net backscatter increase.

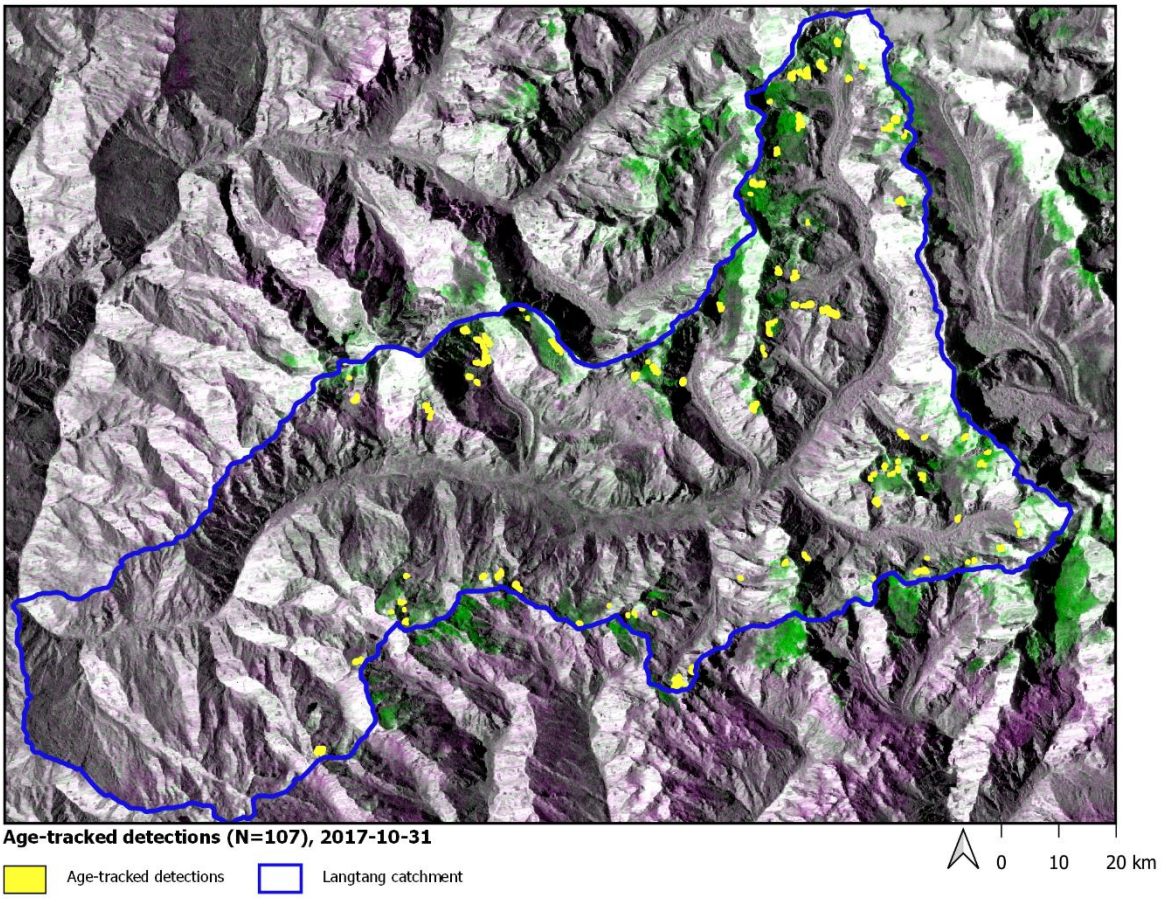

Figure 19: RGB change detection image from 31 October 2017 with age-tracked detections superimposed.

A similar case to the situation from 31 October 2017, resulting in a high false alarm rate, is shown in Figure 20. Between 18 and 22 April 2017, the snow at high elevations turned wet (quantitative statement, percent water in the snow unknown), seen by the purple colors. 4 May 2017 the snow tried up or potentially disappeared leading to a relative increase in backscatter at the locations where wet snow was detected previously. This led to a number of false alarms as seen in the lower right panel of Figure 20.

2017-04-18	2017-04-22
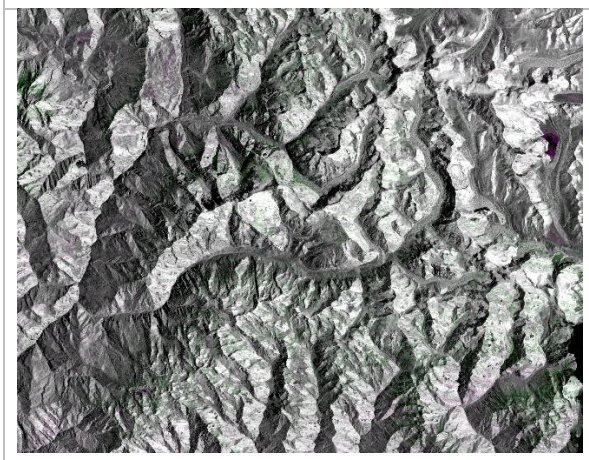	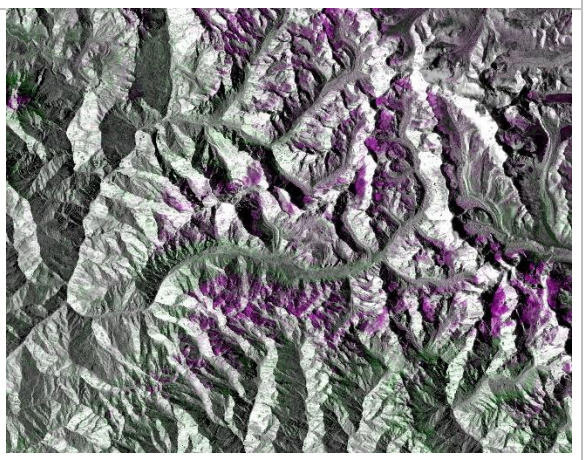

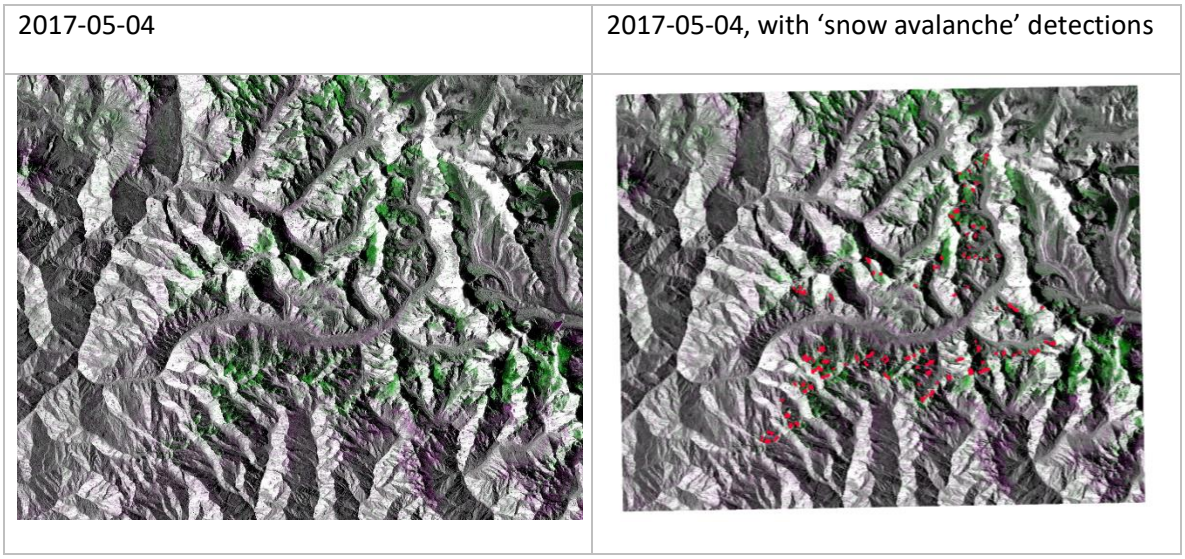

Figure 20: Time series of RGB composites showing changes in snow conditions and resulting feature detection.

In Figure 21 we show examples of snow avalanches. Snow avalanches are manually detectable as green features that extend from the mountain slopes downslope. The pink color tones imply wet snow. Wet snow avalanches are favorable for detection since the relative backscatter contrast between snow avalanche debris, exhibiting an increase in backscatter and surrounding snowpack exhibiting a decrease in backscatter, is large.

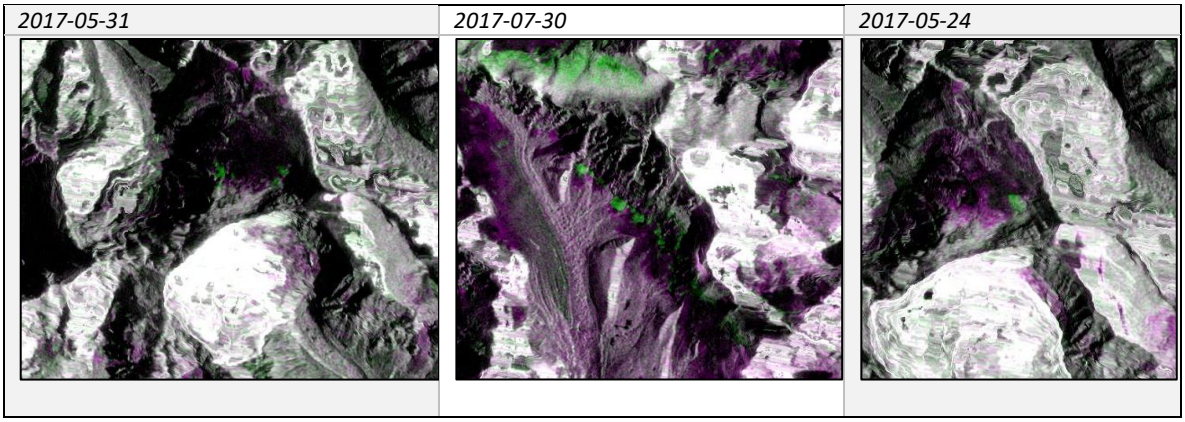

Figure 21: Examples of snow avalanches, visible as green features.

3.5. Comparison of age-tracked detections to ERA5 meteorological variables

For a better understanding of the meteorological conditions in Langtang, we downloaded ERA5 data. We used two grid cells (0.25 x 0.25 degrees lat/long) that cover the Langtang catchment and averaged the 6h data over the area. We visually compared age-tracked detections and their minimum elevation with air temperature, snow depth and precipitation (example for 2017 in Figure 22, the others years are shown in the appendix).

Before going into an analysis, it should be noted that ERA5 is most likely less ideal for an understanding of meteorological conditions in an area with high topographic relief. We would think that ERA5 is fine for estimating precipitation unless there is some high-resolution downscaled model used. Temperature and snow depth are more of a problem since we do not know the geopotential height of the grid cells used for data download. However, ERA5 gives us an indication of when there is snow in the landscape, what the general temperature regime is and how wet or dry the area is.

With regards to snow avalanche activity, however, this exercise raised more questions than answers. We are wondering for example why the monsoon season in JJA, with maximum amounts of precipitation does not result in more detectable snow avalanche activity? Do temperatures at high grounds reach above freezing at all, or can we expect wet snow avalanches as well, particularly in spring and summer? Or is the solar insulation and sublimation such strong drivers of snow melt that we barely would expect snow avalanche activity.

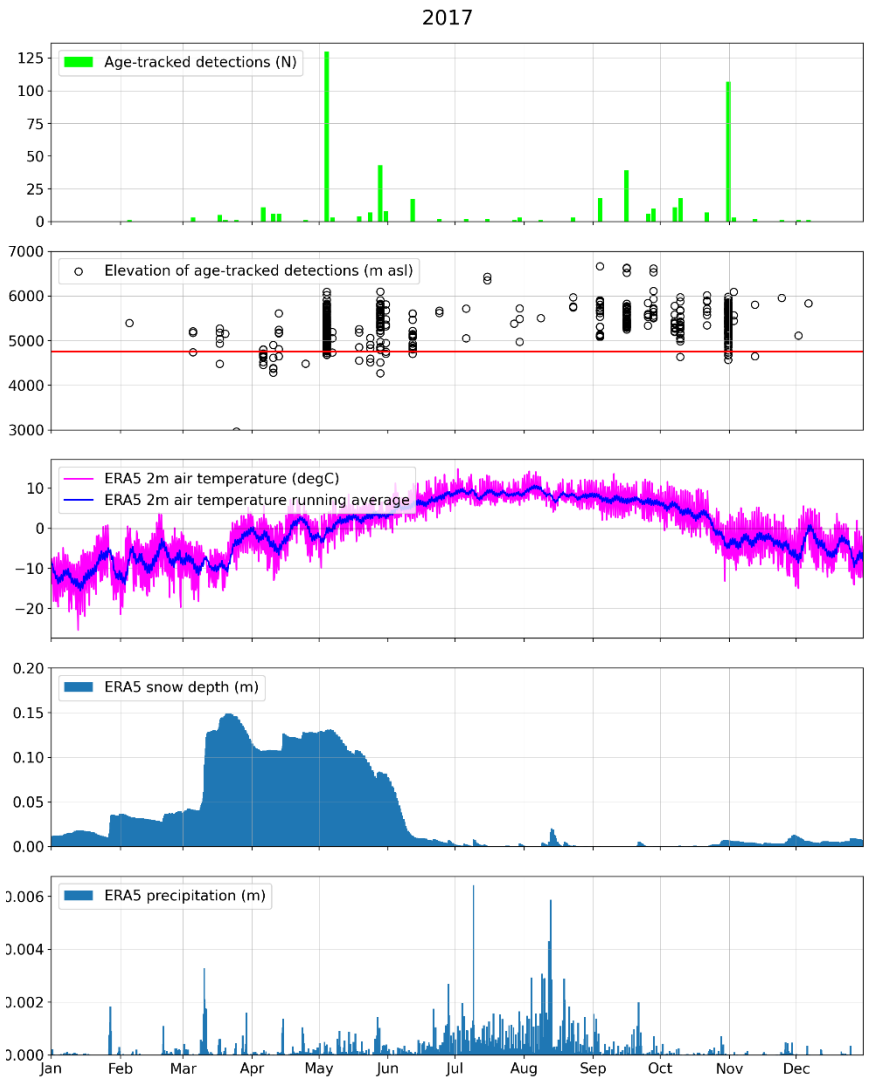

Figure 22: Time series of age-tracked detections from 2017 compared to ERA5 meteorological values.

4. Discussion and conclusion

4.1. From detections to snow avalanche activity and the problem of false positives

Our snow avalanche detector searches for localized backscatter increase above a dynamic threshold that is calculated from the net relative backscatter increase that takes place between two Sentinel-1 images. The detector has no knowledge about how snow avalanche debris typically looks like or where it occurs. The avalanche runout mask confines detections to areas where the occurrence of snow avalanche debris is most likely, thereby increasing our certainty that the detections are snow avalanches.

However, for C-band SAR (sensor frequency on board the Sentinel-1's), dry snow is transparent. This means that even though a detection is within the avalanche runout mask, it is not necessary a snow avalanche. We are therefore dependent on knowing the snow coverage and snow dynamics in the area. The MODIS snow cover products were only to a certain degree helpful and at least the SLC gave an indication of a periglacial environment from roughly 4750 m and up (Figure 15). At these elevations, we would expect snow avalanche activity to occur year-round. Considering ERA5 data does not solve the puzzle for us either and leaves us with more questions about when, which type of snow avalanche can be expected in any given year. A study from the western Himalayas (Ballesteros-Cánovas et al., 2018) hints at high snow avalanche activity mostly in the period January – March, however, we are unsure if this also applies to the Langtang catchment.

To sum up our analysis thus far, visual checks, the elevation dependency of the detections as well as their general timing in the year suggest that the age-tracked detections are likely snow avalanches. However, there is unfortunately a large exception for most days with 100+ detections. These mostly occurred both when there seemed to be a shift in air temperature above and below freezing in spring and autumn respectively causing very high false alarms due to extensive areas that experienced relative backscatter increase.

The other large uncertainty, that we tried to tackle by improving our understanding of snow dynamics and meteorological conditions has to do with the question of how many snow avalanches and when are we simply not detecting? As mentioned further above are we worried about the lack of detections during the summer months for example. We are also aware that even large, dry powder snow avalanches are likely not detectable since they usually do not deposit detectable snow avalanche debris. If the Langtang catchment has first and foremost a dry powder snow avalanche regime, our method is critically limited in quantifying that regime.

4.2. Snow avalanche activity monitoring using Sentinel-1 in Langtang, Nepal

The use satellite-borne SAR data in terms of sensor resolution, spatio-temporal coverage radar bandwidth and detection method depends on the monitoring case. We sum up several monitoring cases in Table 1 with associated recommendation of the spatial resolution, recommended SAR sensor, detection method and processing system.

20 m spatial resolution SAR images provided freely available by Sentinel-1 is always a good choice and the only feasible option if an entire event history (2014 – present) or near-real time monitoring are the monitoring cases of interest. For smaller areas, the Sentinel-1 IW mode data can also be geocoded with 10 m resolution, slightly increasing speckle, however, also increasing detection accuracy. For these systematic monitoring cases, our SATSKRED processing system, using an automatic detector, is recommended. Another processing system, that is currently developed by NORCE is provided via ESA's Geohazard Thematic Platform (https://geohazards-tep.eu/). For some costs, snow avalanche detections can be requested from anywhere globally. However, the data is not quality checked or validated. For event-based studies, very high-resolution SAR data, for example from TerraSAR-X or Radarsat-2 can be used and have been successfully tested by NORCE. However, these data come with a significant cost and are not always available for the area and time of interest. Finally, for event-based studies, SAR data could be processed using for example Google Earth Engine (Gorelick et al., 2017) and scripts provided by Vollrath et al. (2020) for radar shadow and layover mask creation.

Table 1: Snow avalanche activity monitoring cases and recommended methods.

Monitoring case	Recommended spatial resolution	Recommended SAR sensor	Recommended detection method	Recommended processing system
Regional case studies and cycles	1 - 20 m	Sentinel-1 IW, Radarsat-2 UF, TerraSAR-X spotlight	Manual interpretation or automatic detection	SATSKRED, GEE (Google Earth Engine), GEP (Geohazard Thematic Platform)
Avalanche path case studies	1 – 20 m	Sentinel-1 IW, Radarsat-2 UF, TerraSAR-X spotlight	Manual interpretation or automatic detection	SATSKRED, GEE, GEP
Regional or avalanche path event history	10 – 20 m	Sentinel-1 IW	Automatic detection	SATSKRED, GEP
Near-real time monitoring of region or avalanche path	20 m	Sentinel-1 IW	Automatic detection	SATSKRED, GEP

4.3. Snow avalanche regime of Langtang, Nepal

From the snow avalanche detection and the comparison to meteorological variables, we infer some qualitative statements on the snow avalanche regime of Langtang, Nepal. A description of a snow avalanche regime considers the spatio-temporal patterns of snow avalanche activity and their most likely meteorological and snowpack triggers. This synthesis than often builds the basis for the design of qualitative analysis of which factors trigger snow avalanches as well as appropriate hazard management strategies such as repeated regional snow avalanche forecasting or active (e.g. snow avalanche control by explosives) and permanent mitigation measures (e.g. deflection dams in the runout zone or snow support structures in the starting zone).

The Langtang catchment seems to be a semi-arid high mountain valley that experiences minor snowfall in general with a strong altitudinal gradient towards more snow at high elevations and only a couple of days of snow fall in the lower lying valley bottom. Sun insolation might play an important role in determining where snow remains for extended periods, as well as when the onset of snowmelt takes place. It is thus likely that snow avalanches trigger at high elevations and run on bare ground at some point in the avalanche path, also entraining rock debris and sediment. It is also likely that snow avalanches that start at high elevations become airborne when falling over cliffs, turning into dry powder snow avalanches. In both cases, the depositions likely contain minor amounts of snow. Nevertheless, both rock debris and the impact pressure of the powder cloud can cause substantial damage. Dynamic avalanche modelling would quantify the impact pressures and maximum runout of these snow avalanches.

We then believe that the snow avalanche regime is event-based, meaning that infrequent, large, destructive snow avalanches dominate snow avalanche activity and are also responsible for the main hazard. Likely triggers of such destructive snow avalanches are heavy snow loading events, especially also due to wind redistribution of snow, serac falls or calving events from ice cliffs.

In terms of hazard management, we recommend extending the Sentinel-1 borne detection of snow avalanches to increase the temporal extend of the snow avalanche activity data series. We further recommend decreasing the uncertainty in Sentinel-1 borne detections by comprehensive field validation. This dataset could then build the basis for an analysis of which synoptic-scale weather patterns cause either destructive snow avalanches or large snow avalanche cycles and how these synoptic -scale patterns manifest in meteorological conditions on site. In areas where data is sparse, a synoptic meteorological analysis is usually highly recommended.

References

Ballesteros-Cánovas, J.A., Trappmann, D., Madrigal-González, J., Eckert, N., Stoffel, M., 2018. Climate warming enhances snow avalanche risk in the Western Himalayas. Proc. Natl. Acad. Sci. 115, 3410–3415. https://doi.org/10.1073/pnas.1716913115

Bianchi, F.M., Grahn, J., Eckerstorfer, M., Malnes, E., Vickers, H., 2020. Snow avalanche segmentation in SAR images with Fully Convolutional Neural Networks. IEEE J. Sel. Top. Appl. Earth Obs. Remote Sens. 1–1. https://doi.org/10.1109/JSTARS.2020.3036914

Bühler, Y., Hafner, E.D., Zweifel, B., Zesiger, M., Heisig, H., 2019. Where are the avalanches? Rapid SPOT6 satellite data acquisition to map an extreme avalanche period over the Swiss Alps. The Cryosphere 13, 3225–3238. https://doi.org/10.5194/tc-13-3225-2019

Eckerstorfer, M., Malnes, E., 2015. Manual detection of snow avalanche debris using high-resolution Radarsat-2 SAR images. Cold Reg. Sci. Technol. 120, 205–218. https://doi.org/10.1016/j.coldregions.2015.08.016

Eckerstorfer, M., Vickers, H., Malnes, E., Grahn, J., 2019. Near-Real Time Automatic Snow Avalanche Activity Monitoring System Using Sentinel-1 SAR Data in Norway. Remote Sens. 11, 2863. https://doi.org/10.3390/rs11232863

Gorelick, N., Hancher, M., Dixon, M., Ilyushchenko, S., Thau, D., Moore, R., 2017. Google Earth Engine: Planetary-scale geospatial analysis for everyone. Remote Sens. Environ., Big Remotely Sensed Data: tools, applications and experiences 202, 18–27. https://doi.org/10.1016/j.rse.2017.06.031

Hafner, E.D., Techel, F., Leinss, S., Bühler, Y., 2020. Mapping avalanches with satellites – evaluation of performance and completeness. Cryosphere Discuss. 1–31. https://doi.org/10.5194/tc-2020-272

Khadka, N., Khadka, N., Ghimire, S.K., Chen, X., Thakuri, S., Hamal, K., Shrestha, D., Sharma, S., 2020. Dynamics of Maximum Snow Cover Area and Snow Line Altitude Across Nepal (2003-2018) Using Improved MODIS Data. J. Inst. Sci. Technol. 25, 17–24. https://doi.org/10.3126/jist.v25i2.33729

Larsen, H.T., Hendrikx, J., Slåtten, M.S., Engeset, R.V., 2020. Developing nationwide avalanche terrain maps for Norway. Nat. Hazards. https://doi.org/10.1007/s11069-020-04104-7

Larsen, Y., Engen, G., Lauknes, T.R., Malnes, E., Høgda, K.A., 2005. A generic differential interferometric SAR processing system, with applications to land subsidence and snow-water equivalent retrieval, in: ESRIN, E. (Ed.), . Presented at the Fringe ATSR Workshop 2005, p. 6.

Leinss, S., Wicki, R., Holenstein, S., Baffelli, S., Bühler, Y., 2020. Snow avalanche detection and mapping in multitemporal and multiorbital radar images from TerraSAR-X and Sentinel-1. Nat. Hazards Earth Syst. Sci. 20, 1783–1803. https://doi.org/10.5194/nhess-20-1783-2020

Lied, K., Bakkehøi, S., 1980. Empirical calculations of snow avalanche run-out distances based on topographic parameters. J. Glaciol. 26, 165–177.

Muhammad, S., 2020. Improved daily MODIS TERRA/AQUA Snow and Randolph Glacier Inventory (RGI6.0) data for High Mountain Asia (2002-2019). https://doi.org/10.1594/PANGAEA.918198

Muhammad, S., Thapa, A., 2020. An improved Terra–Aqua MODIS snow cover and Randolph Glacier Inventory 6.0 combined product (MOYDGL06*) for high-mountain Asia between 2002 and 2018. Earth Syst. Sci. Data 12, 345–356. https://doi.org/10.5194/essd-12-345-2020

Oterhals Daugstad, H., n.d. Validation of satellite-detected snow avalanches by records from avalanche control work around Tyin, Norway. University of Oslo, Oslo, Norway.

Sinha, S., Giffard-Roisin, S., Karbou, F., Deschatres, M., Karas, A., Eckert, N., Coléou, C., Monteleoni, C., 2019. Can Avalanche Deposits be Effectively Detected by Deep Learning on Sentinel-1 Satellite SAR Images?, in: Climate Informatics. Paris, France.

Vickers, H., Eckerstorfer, M., Malnes, E., Doulgeris, A., 2017. Synthetic Aperture Radar (SAR) Monitoring of Avalanche Activity: An Automated Detection Scheme, in: Sharma, P., Bianchi, F.M. (Eds.), Image Analysis. Springer International Publishing, Cham, pp. 136–146. https://doi.org/10.1007/978-3-319-59129-2_12

Vollrath, A., Mullissa, A., Reiche, J., 2020. Angular-Based Radiometric Slope Correction for Sentinel-1 on Google Earth Engine. Remote Sens. 12, 1867. https://doi.org/10.3390/rs12111867

Waldeland, A.U., Reksten, J.H., Salberg, A.-B., 2018. Avalanche Detection in Sar Images Using Deep Learning. Presented at the IGARSS 2018 - IEEE International Geoscience and Remote Sensing Symposium. https://doi.org/10.1109/IGARSS.2018.8517536

5. Appendix

List of parameters that are attached to the snow avalanche vectors as attribute table:

FID – unique number id
Shape – polygon (similar for all)
OBJECTID – running number
area – area of detected avalanche in square meters
aspect – currently not computed (we are working on it)
det_count – always set at 1
east – x coordinates
length – maximum length of the polygons (not parallel to avalanche path)
north – y coordinates
raster_val – number of detected pixels
refdate – same as T_0
sat_geom – satellite track number
t_0 - reference date (used for constructing change detection images)
t_1 - activity date (date of avalanche detection)
time – same as t_1
track_id – for our use only
uuid – for our use only
width – not computed right now
dem_mean – mean elevation of entire polygon
dem_median – median elevation of entire polygon
dem_min – longest runout (m asl of pixel)
dem_max – furthest upslope position (m asl of pixel)
slp_mean – mean slope angle of entire polygon
slp_min – min slope angle of entire polygon
slp_max – max slope angle of entire polygon
vv1… - backscatter parameters

Table 2

	CATCHMENT	RUNOUT	RADARMASK_121	RADARMASK_085	RADARMASK_019
SQUAREM	585,387,600	328,067,200	258,255,600	286,027,600	256,912,800
PIXEL COUNT	1460974	820168	645639	715069	642282

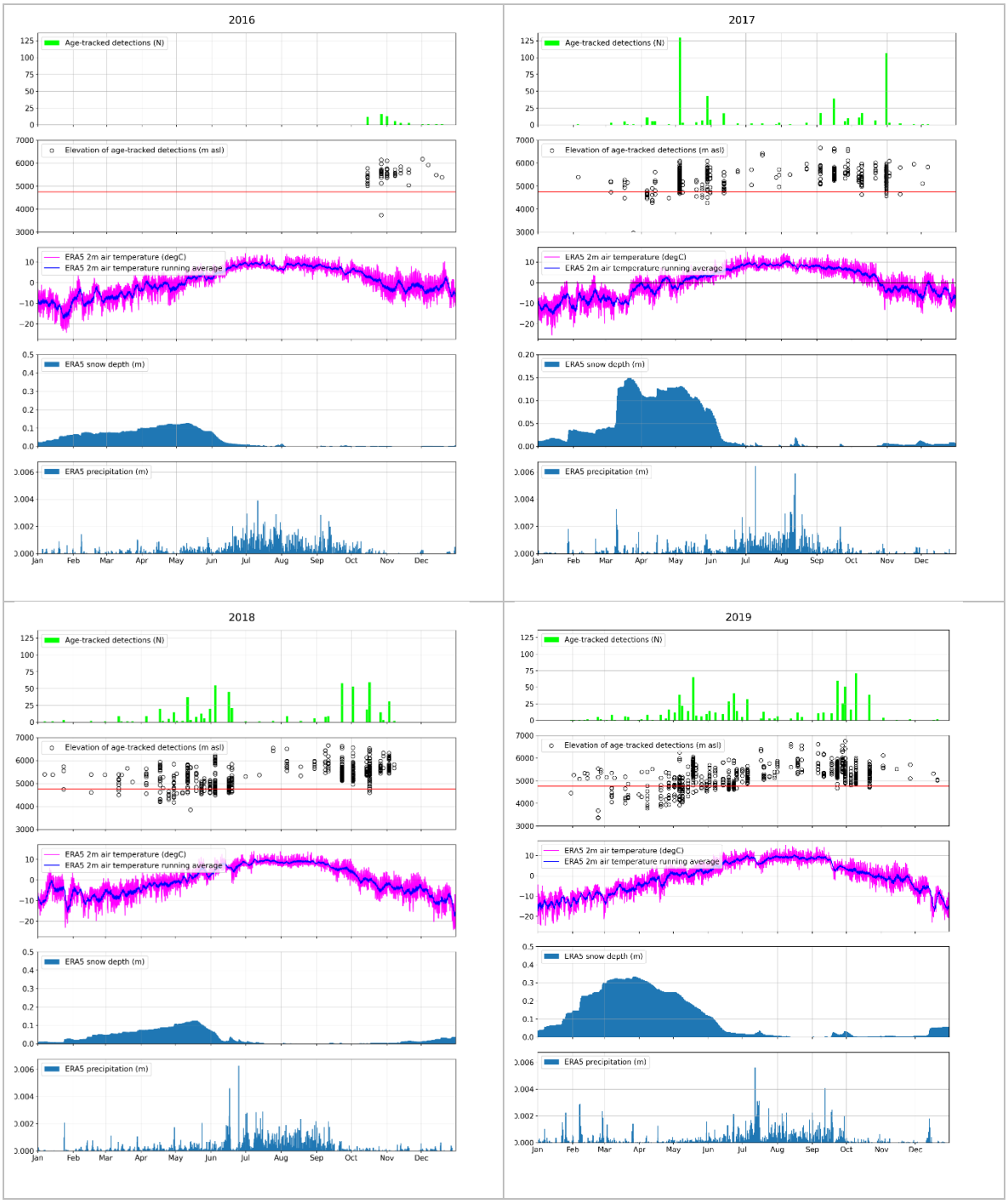
2016
2017
2018
2019
Age-tracked detections (N)
Elevation of age-tracked detections (m asl)
ERA5 2m air temperature (degC)
ERA5 2m air temperature running average
ERA5 snow depth (m)
ERA5 precipitation (m)
Jan Feb Mar Apr May Jun Jul Aug Sep Oct Nov Dec

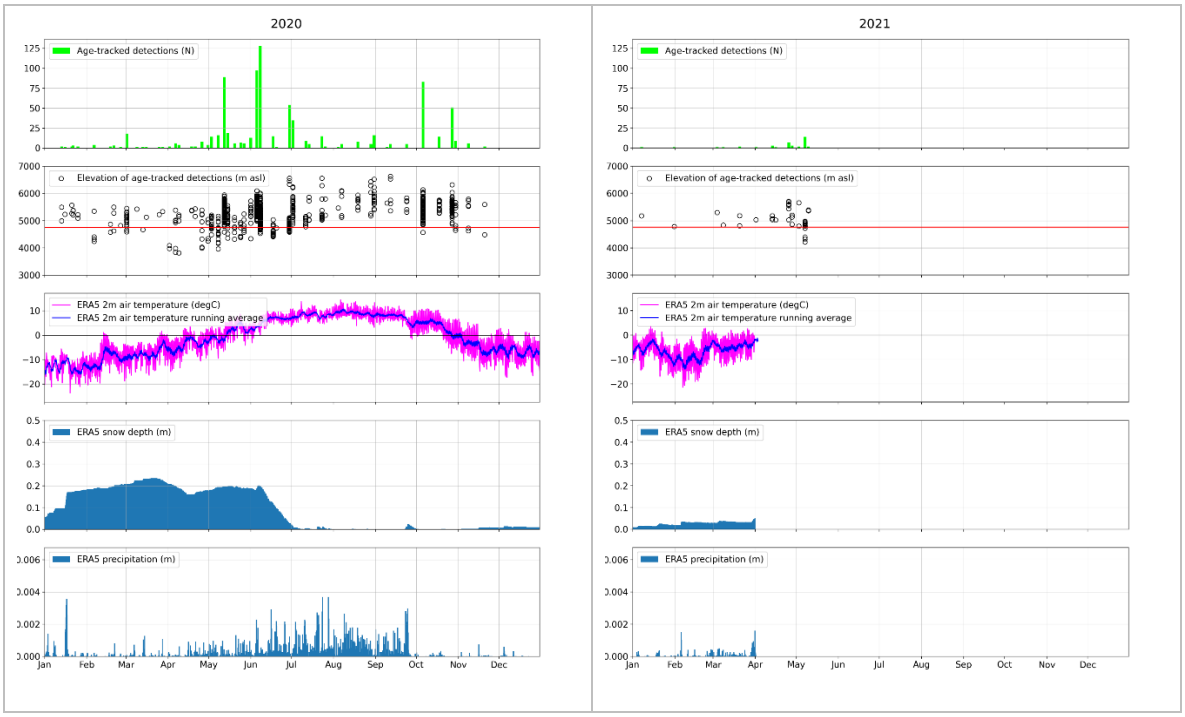
2020
2021
Age-tracked detections (N)
Elevation of age-tracked detections (m asl)
ERA5 2m air temperature (degC)
ERA5 2m air temperature running average
ERA5 snow depth (m)
ERA5 precipitation (m)
Jan
Feb
Mar
Apr
May
Jun
Jul
Aug
Sep
Oct
Nov
Dec

Figure 23